

ARTICLE

Solar light active flexible activated carbon cloth-based photocatalyst for Markovnikov-selective radical-radical cross-coupling of *S*-nucleophiles to terminal alkyne and liquefied petroleum gas sensing

Pooja Singh¹ | Rajesh K. Yadav¹  | Tae Wu Kim²  | Tara C. Yadav³ |
 Vitthal Gole⁴ | Abhishek K. Gupta⁵ | Kuldeep Singh⁶ | Kuldeep Kumar⁷ |
 Bal Chandra Yadav⁷ | D. K. Dwivedi⁵

¹Department of Chemistry and Environmental Science, Madan Mohan Malaviya University of Technology, Gorakhpur, India

²Department of Chemistry, Mokpo National University, Muan-gun, Jeollanam-do, Republic of Korea

³Department of Biotechnology, Indian Institute of Technology Roorkee, Roorkee, India

⁴Department of Chemical Engineering, Madan Mohan Malaviya University of Technology, Gorakhpur, India

⁵Department of Physics and Material Science, Madan Mohan Malaviya University of Technology, Gorakhpur, India

⁶BRD Medical College, Gorakhpur, India

⁷Nanomaterials and Sensors Research Laboratory, Department of Physics, Babasaheb Bhimrao Ambedkar University, Lucknow, India

Correspondence

Rajesh K. Yadav, Department of Chemistry and Environmental Science, Madan Mohan Malaviya University of Technology, Gorakhpur-273010, Uttar Pradesh, India.
 Email: rajeshkr_yadav2003@yahoo.co.in

Tae Wu Kim, Department of Chemistry, Mokpo National University, Muan-gun, Jeollanam-do, 58554, Republic of Korea.
 Email: twkim@mokpo.ac.kr

Abstract

Selective radical-radical coupling of terminal alkynes and thiol has been broadly used in chemical synthesis, providing plausible entries to the formation of anti-Markovnikov products. Because of the selective control and Kharasch effect, the formation of Markovnikov products still remains an immense challenge. Herein, we designed a covalent organic polymer, poly(naphthalene 1,4,5,8-tetracarboxylic dianhydrideimide-benzoquinone) through in situ polymerization on activated flexible carbon cloth to function as a light harvester material for selective Markovnikov radical-radical coupling of terminal alkynes and thiol. Mechanistic explorations verified that cross-coupling between radical of terminal alkynes and thiol might be the key route in this organic transformation, such as C–S bond formation. This selective radical-radical Markovnikov of cross-coupling protocol provide an opportunity to assist the synthesis of valuable vinyl sulfide. Additionally, the synthesized material has been explored as liquefied petroleum gas (LPG) sensor for 0.5, 1.0, 1.5, and 2.0 vol% LPG, respectively. At 2.0 vol% LPG, it shows maximum sensor response as 635.29. Least response and recovery times are 2.44 and 1.0 s, respectively.

KEYWORDS

cross coupling, cyclic voltammetry, photocatalysis

1 | INTRODUCTION

Radical/radical cross coupling between terminal alkynes and thiols have long served as potential techniques to access complex molecules.^[1] In this situation, exclusively anti-Markovnikov products were achieved due to the various effects such as Kharasch effect.^[1,2] Accordingly, techniques allowing for direct highly efficient synthesis of α -substituted vinyl derivatives from cross-coupling radical of terminal alkynes and sulfonyl derivatives have infrequently been reported.^[3] In the literature, generated the stable radical intermediate from the radical/radical cross-coupling step is the key for the ultimate selectivity control, and addition of anti-Markovnikov often provides the utmost stable radical intermediate (Scheme 1a). Therefore, seeking a new route to synthesize solar light-based valuable α -substituted fine chemicals such as vinyl compounds through radical/radical Markovnikov cross-coupling procedure is interesting and tremendously challenging. Inspired by the state of the art of radical/radical cross coupling,^[4] we wondered whether the Markovnikov products, α -substituted vinyl derivatives, can be achieved through the general and useful cross-coupling of the radical, a vinyl carbon, and other organic sulfide radicals (Scheme 1b).

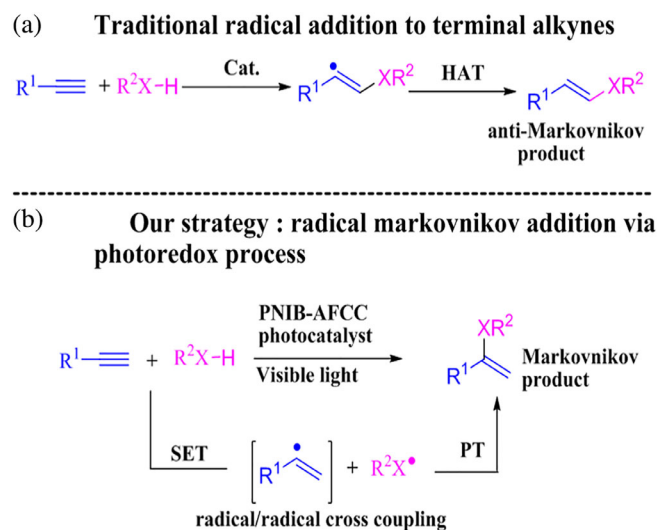
According to the abovementioned concept, α -substituted vinyl sulfides, which are not only used in biological science, medicinal, and pharmaceutical chemistry^[5] but also serve as useful synthetic intermediates,^[6] were selected as synthetic target molecules. An enlargement of synthetic approach to vinyl derivative organic compounds has received important attention in recent

years.^[7] Till date, the majority of synthetic methods for the preparation of vinyl derivative organic compounds lead to β -substituted useful organic products.^[7,8] Nevertheless, the synthesis of α -substituted vinyl sulfides, which have excellent potential application in pharmaceutical science^[9–13] still remains a key challenge. Traditionally, expensive noble transition metal catalysts are used to the synthesis of α -substituted vinyl organic compounds with poor selectivity as per established approaches.^[14–19] An alternative strategy with environmentally friendly, more simple, economical, and sustainable perspective is therefore highly interesting. Recently, solar light active photoredox catalysis has become a powerful tool for the development of a wide range of radical/radical cross-coupling under mild conditions.^[20–22] Thus, we imagined that solar light active photocatalysis might enable access to α -substituted vinyl sulfides through radical/radical cross-coupling processes. Herein, we report on the synthesis and development of a covalent organic polymer (COP), poly (naphthalene 1,4,5,8-tetracarboxylic dianhydrideimide-benzoquinone) (see Figure S1) through in situ polymerization on activated flexible carbon cloth (PNIB-AFCC) (Scheme 2) to function as a light harvester material for selective Markovnikov radical-radical cross-coupling of terminal alkynes and thiols. A wide range of α -substituted vinyl sulfides can be achieved with exclusive Markovnikov regioselectivity.

2 | RESULTS AND DISCUSSION

X-ray diffraction (XRD) analysis of T, N, and PNIB-AFCC photocatalyst is shown in Figure 1. The XRD analysis of T and N reveals a small weak peak at 2θ value of 8° , and 15° , respectively. A shift in the scattering weak and broad peaks to near about 14° in the XRD pattern of PNIB-AFCC photocatalyst may be recognized to T covalently attached to N, which indicates that imides bond formation between the amino group of T and anhydride gp of N and also broad peak of PNIB-AFCC show the polymeric nature of photocatalyst and π - π stacking between AFCC and PNIB photocatalyst.^[23]

The UV-visible absorption spectra of PNIB, PNIB-AFCC photocatalysts are shown in Figure S2. The absorption spectrum of PNIB-AFCC photocatalyst reveals at 430 nm. PNIB shows lower absorption at 430 nm while PNIB-AFCC shows higher absorption in the same range. The optical band gap of PNIB-AFCC photocatalyst is 2.63 eV. The optical band gap of PNIB photocatalyst is nearly the same as the calculated band gap (2.5 eV) by cyclic voltametric study (Figure S3). The shift of absorption maxima in PNIB-AFCC photocatalyst compared with that in PNIB indicates the strong π - π interaction



SCHEME 1 (a) C–S bond formation on terminal alkyne via anti-Markovnikov addition. (b) C–S bond formation on terminal alkyne via Markovnikov addition. PT, proton transfer

SCHEME 2 Synthesis of PNIB-AFCC photocatalyst with T, N, and AFCC via in situ polymerization method

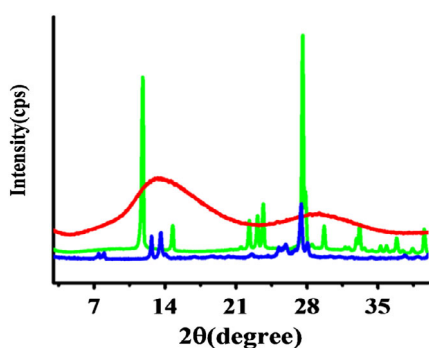
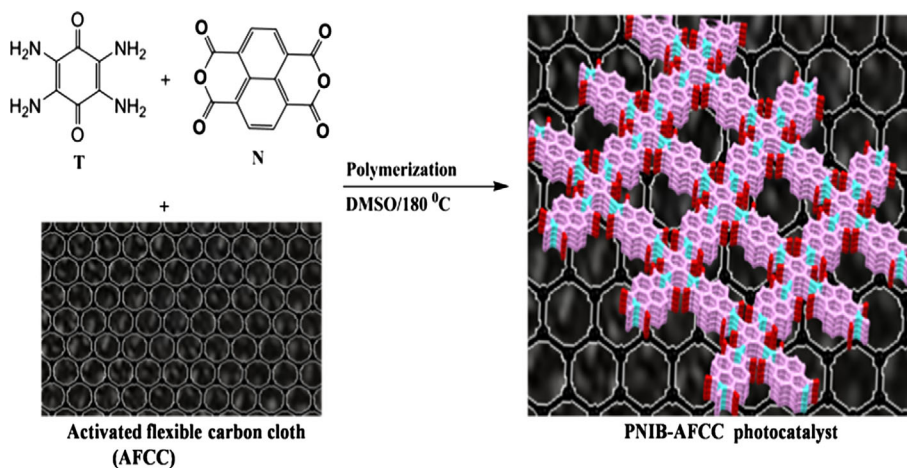


FIGURE 1 XRD analysis of PNIB-AFCC (red), T (blue), and N (green)

between AFCC and PNIB photocatalyst which is highly suitable for the C–S bond formation under solar light irradiation.^[24–25]

The 3D structure and surface morphology of PNIB and PNIB-AFCC photocatalysts are shown in Figure 2. Surface morphology of PNIB and PNIB-AFCC photocatalysts is explained with the help of atomic force microscopy (AFM) analysis (Figure 2b,c). The samples for AFM analysis were prepared by drop-casting ultrasonic treatment of PNIB and PNIB-AFCC in *N,N*-dimethylformamide (DMF) (0.00027 g/L) on an unsoiled glass surface. The topographic average roughness of flexible PNIB and PNIB-AFCC was found to be 2.84 and 3.94 nm, respectively (Figure 2b,c). The surface height of PNIB-AFCC was higher than PNIB photocatalyst, which indicates that PNIB is covered on the edge of AFCC and also confirms the strong π – π interaction between AFCC and PNIB.^[25,26]

The morphology of the N, T, PNIB and PNIB-AFCC photocatalysts was also investigated by field-emission scanning electron microscopy. Figure S4 shows the morphology of T and N which is layered and rod shaped, respectively. Furthermore, the morphology of PNIB

photocatalyst is entirely different from the morphology of T and N moieties, due to the covalently attachment of T and N materials. Finally, the morphology of PNIB-AFCC photocatalyst is completely different from the PNIB photocatalyst morphology, due to the edge of AFCC covered by PNIB and also confirms the strong π – π interaction between AFCC and PNIB (Figure 3).^[27,28]

Dynamic light scattering technique shows the average particle size of N, PNIB, and PNIB-AFCC photocatalysts (see Figure S5). The particle sizes of N, PNIB, and PNIB-AFCC are 1,000, 400, and 250 nm respectively. The particle size is one of the significant factors for the photocatalytic activity of photocatalyst in organic transformation. According to the previous study,^[29] small particles have the high surface area associated with the multi-electron collector capacity of incoming light on PNIB-AFCC, which facilitates the increase of electron transfer rate on the surface of PNIB-AFCC photocatalyst.^[30]

Rapidly light-scattering techniques were used for measuring the zeta potential values of PNIB-AFCC and PNIB. The zeta potential of PNIB-AFCC is 0.0665 mV which is less than the zeta potential value of PNIB 0.515 mV (see Figure S6). The less value of PNIB-AFCC is indicating the strong π – π interaction between AFCC and PNIB photocatalyst.^[31]

The covalent attachment of T and N for the formation PNIB and PNIB-AFCC photocatalysts was characterized by Fourier transform infrared (FTIR) spectroscopy as shown in Figure 4a. The FTIR spectra of N (see Figure S7) shows strong peak at 1,773 cm^{-1} due to the dianhydride carbonylic group and T shows stretching vibration peak at 1,605 cm^{-1} of C=O gp of quinone.^[32,33] After attachment of T and N, a new peak was observed in the spectrum of PNIB photocatalyst (see Figure S13) at 1,720 cm^{-1} which is corresponding to the C=O stretching band of the imide group.^[34]

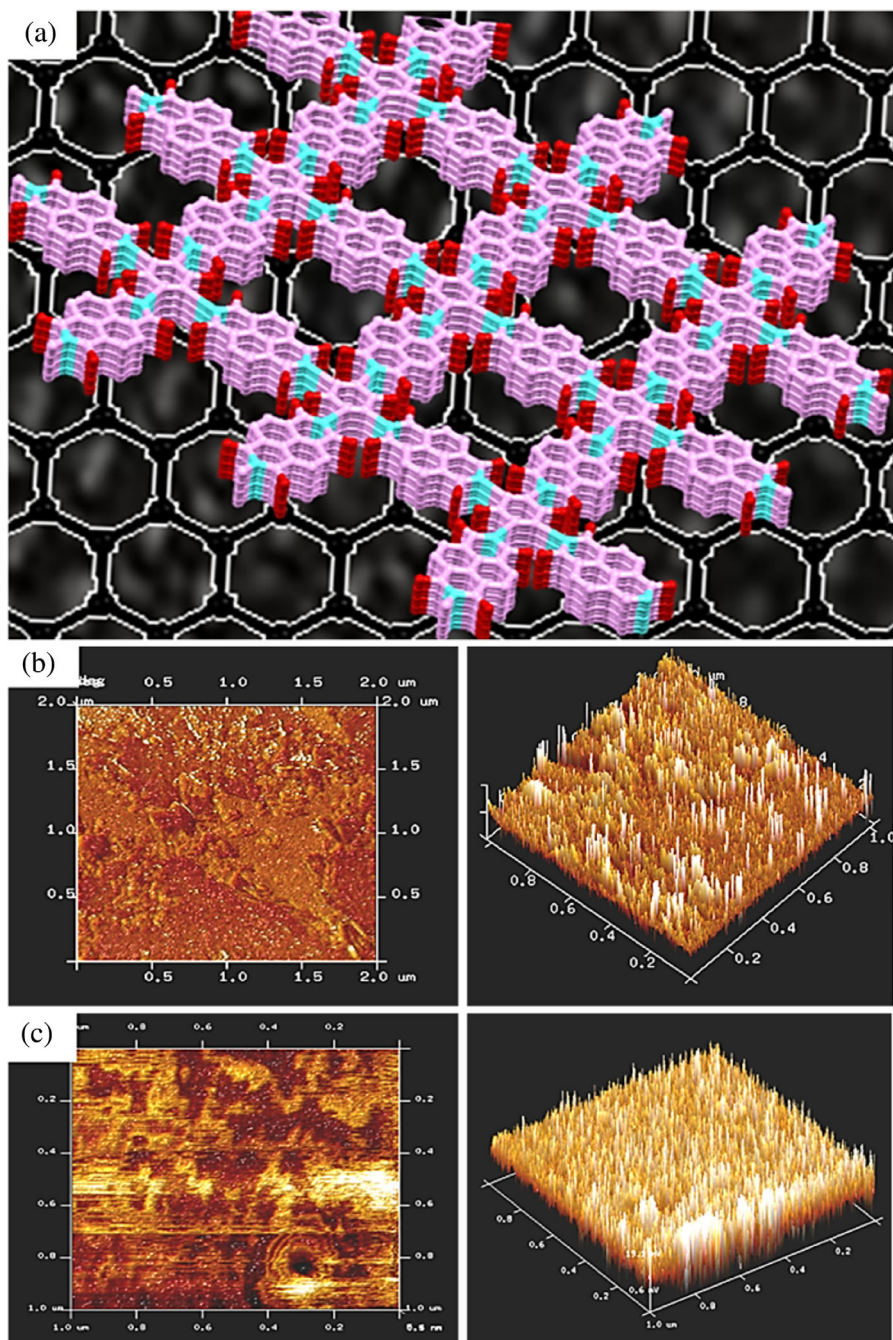


FIGURE 2 (a) 3D structure of the PNIB-AFCC photocatalyst, along with AFM roughness and 3D images of (b) PNIB and (c) PNIB-AFCC photocatalysts, respectively

The thermal behavior of N, PNIB, and PNIB-AFCC photocatalysts was investigated in the range of temperature 25–900°C at a heating rate 10°C/min under nitrogen flow by different techniques such as thermogravimetric analysis (TGA), differential thermal analysis (DTA), and derivative thermogravimetry (DTG) analysis. The PNIB and PNIB-AFCC photocatalysts displayed slow weight loss with increase temperature up to 900°C. The next weight loss of PNIB, PNIB-AFCC photocatalysts started with 200°C and ended with 500°C with weight loss 57.2 and 45.4% which indicates the dissociation of imides bond of PNIB and PNIB-AFCC photocatalysts,^[35]

respectively, as shown in Figure 4b. Further, last weight loss of PNIB at 600°C is 30.0% and PNIB-AFCC at 615°C is 15.8% which shows that the PNIB-AFCC photocatalyst is thermally more stable than the PNIB photocatalyst. The TGA analysis was conducted for N in nitrogen atmosphere. The achieved results show that no significant weight loss was observed before near about 385°C for N, showing good thermal stability. Upon further heating, the N sample starts to decompose (Figure 4b).

DTA analysis also explains the thermal behavior of N, PNIB, and PNIB-AFCC photocatalysts. In Figure 5a, the broad exothermic peak of N near about at

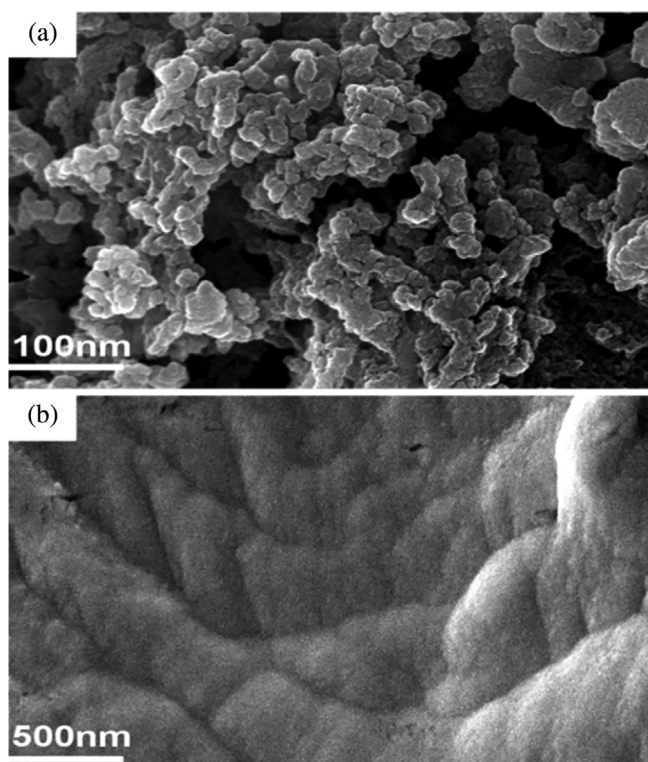


FIGURE 3 Field-emission scanning electron microscopy (FESEM) images of (a) PNIB and (b) PNIB-AFCC photocatalysts

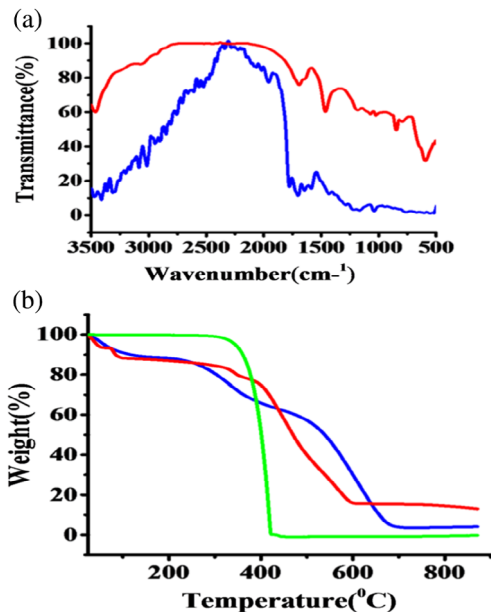


FIGURE 4 (a) FTIR analysis of PNIB-AFCC (red), PNIB (blue), and (b) TGA analysis of PNIB-AFCC (red), PNIB (blue) and N (green)

400°C indicates the disintegration of N. The breakages of imide bonds in the PNIB and PNIB-AFCC photocatalysts were started at 589 and 580°C, respectively.

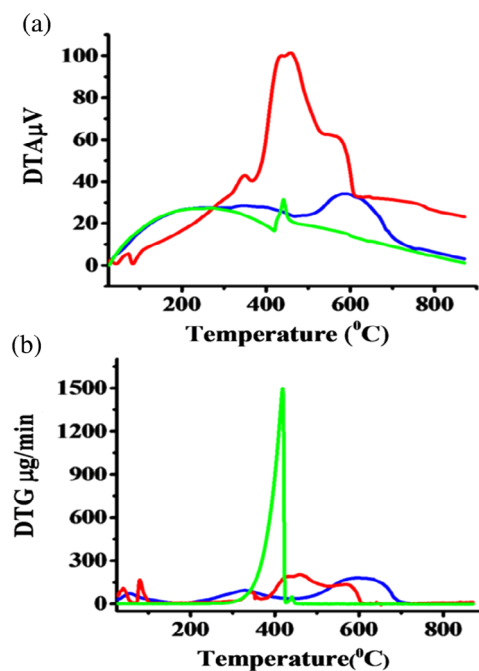


FIGURE 5 (a) DTA analysis of PNIB-AFCC (red), PNIB (blue), and N (green) (b) DTG analysis of PNIB-AFCC (red), PNIB (blue) and N (green)

This results from the DTA measurements indicates that PNIB and PNIB-AFCC photocatalysts are thermally more stable than N.^[36]

Similarly, DTG analysis also confirmed the slow weight loss in N, PNIB, and PNIB-AFCC photocatalysts, exhibiting excellent thermal stability for all samples (Figure 5b). PNIB photocatalyst shows weight loss rate at two stages, first weight loss at 330°C at 0.009 mg/min and second weight loss 0.01856 mg/min at 617°C. In the same way, PNIB-AFCC photocatalyst shows weight loss at 355, 481, 589°C at 0.0829, 0.202, 0.133 mg/min, respectively. On the other hand, N is showing weight loss rate at 416°C at 0.148 mg/min, which shows that PNIB and PNIB-AFCC photocatalysts are thermally more stable than N.^[37]

For preparation of thin film of PNIB-AFCC, spin-coating technique was used. Glass substrates of the dimension $1 \times 1 \text{ cm}^2$ were washed with the distilled water, ethanol, and acetone followed with the ultrasonic cleaning. A dilute solution of PNIB-AFCC was made by dissolving it into the iso-propyl alcohol, stirring at 400 rpm along with heating at 50°C for 2 hr. Sonication for 30 min gave a sol and further, it was spun on glass substrate with the help of vacuum-assisted photo-resist spinner at 800 rpm for 20 s. Later, it was dehydrated on the hot plate for 3 min. The same spin coating and dehydrating processes were again performed two times to obtain the uniform and smooth film. Now the electrodes

on the film were deposited with the help of silver paste and finally this sensing device was ready for the LPG sensor characterization.^[38]

The LPG sensor characterization setup is described in our previous published article.^[39] Experimental setup consists with Keithley Electrometer model no. 6517B, glass chamber, and a computer. Glass chamber consists with the gas outlet knob at the side of the chamber and gas inlet at the top of the chamber which is connected to flow meter of the LPG cylinder. The LPG was exposed to the sensing device in the glass chamber and the corresponding resistance of the sensing material was recorded with the help of Keithley Electrometer.

The sensor response, response-recovery time, and reproducibility are the main parameters of a sensor. The % sensor response of a sensor is defined by Equation (1).^[40]

$$\%SR = \frac{|R_g - R_a|}{R_a} * 100 \quad (1)$$

where R_g is the resistance of sensing element in the presence of the LPG while R_a is the resistance in the presence of air.^[41] Response and recovery times are those times in which sensor output reaches to its 90% of the maximum after the exposing and removing the gas during the response and recovery cycle. The response and recovery time of the sensor were calculated with the exponential growth and decay-fitted data according to Equations (2 and 3), respectively.^[42]

$$R_m = R_0 \exp\left(\frac{-t}{t_{res}}\right) \quad (2)$$

$$R_m = R_0 \left\{ 1 - \exp\left(\frac{-t}{t_{rec}}\right) \right\} \quad (3)$$

Its principle is based on the change in electrical properties of the sensing material when exposed to the gas. The LPG sensing operation is based on the charge transfer between the LPG and sensing material. At the room temperature due to applied electrostatic potential, the equilibrium between the oxygen present on the surface of the sensing material and atmospheric oxygen takes place and forms the ionic oxygen species which are shown by Equations (4) and (5). As the LPG interacts with the sensing material, the formed ionic oxygen captured the electron from the sensing material and as a result the density of the electron decreases which increases the resistance of the sensing material. LPG mainly consists of methane, propane, and butane generally can be written

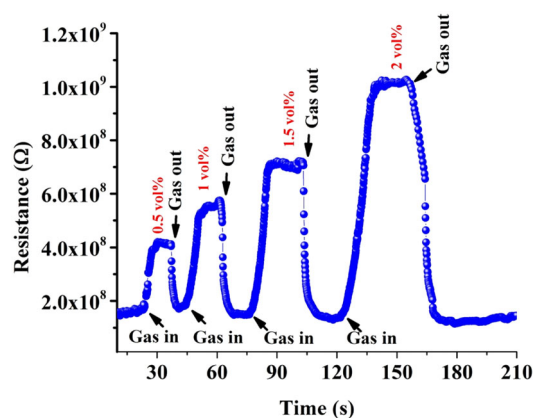
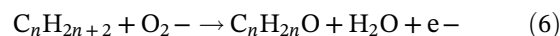
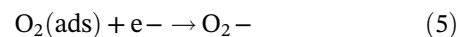
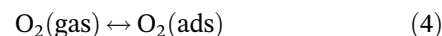


FIGURE 6 LPG sensing characteristics of PNIB-AFCC

as C_nH_{2n+2} . As C_nH_{2n+2} interacted with ionic oxygen species it forms the complex $C_nH_{2n}O$ with water which is shown in Equation (6).



The sensing behavior of PNIB-AFCC-based sensor was studied by applying the voltage of 20 V between the electrodes of the sensing elements. To investigate the gas-sensing characteristics of sensing device, different concentrations of LPG were exposed and the correspondingly different sensing cycles were obtained which are shown in Figure 6. The four sensing cycles represent the variations in the resistance of the sensing material for 0.5, 1.0, 1.5, and 2.0 vol% of LPG, respectively, with respect to time. The resistance of the sensing element in the air was found as $1.70 \times 10^8 \Omega$ and as the 0.5 vol% LPG was exposed inside the chamber; the resistance of sensor was augmented and reached to $4.20 \times 10^8 \Omega$. After that it got saturated. As LPG was exposed, the resistance was found increased and as the outlet was opened, resistance decreased for each cycle. The % sensor response of the sensor was calculated for 0.5, 1.0, 1.5, and 2.0 vol% LPG with the help of Equation (1) and is shown in the Table 1.

In Figure 7a, change in % sensor response with the variations to LPG concentration has been illustrated and this also shows that the sensor has a linear variation in % sensor response with respect to LPG concentration. This characteristic of the sensor is highly considerable for the device fabrication purpose. Figure 7b shows the reproducibility curve for 0.5 vol% of the LPG sensor. The

response and recovery times of the sensor were calculated by the exponential growth and decay fitting for each concentration cycle.

The exponential growth and decay-fitted curves for 1.0 and 0.5 vol% LPG are shown in the Figure 7c,d having response-recovery times as 3.51, 1.00 s, respectively. The calculated response-recovery time for each cycle is shown in Table 1.

The reaction conditions for C–S bond formation were optimized by a mixture of phenyl acetylene (1a) and thiol (thiophenol, 2a), base Na_2CO_3 (1 eq) along with different type of photocatalyst (1 mol%) under solar light illumination.^[43] Using 0.3 mmol of 1a, 0.6 mmol of 2a, and 1 equivalent of Na_2CO_3 in 4 ml DMF along with PNIB as

photocatalyst yielded 82% of the product with 84% conversion of the reactant (Table 2, entry 1). Similarly, when we used starting material T (1 mol%) with 2 equivalents of Na_2CO_3 , 4 ml DMF in 1 hr achieved 26% of the product with 25% conversion of the reactant (Table 2, entry 4). The best product yield of 99% with the conversion of 99% reactant was obtained when we use 1 equivalent of Na_2CO_3 base along with PNIB-AFCC photocatalyst and 4 ml DMF in 1 hr (Table 2, entry 2). As a result, high yield and selectivity was observed upon use of 1 equivalent of Na_2CO_3 in our experiments. After that when we use only AFCC as photocatalyst, no product formation or very less yields of the coupling product (Table 2, entry 4). Combining the all above experiments, we can say that base, photocatalyst, and light are essential components for the formation of the desired coupling product (Table 2, entry 3, and entry 6–7). Herein, in our experiment AFCC enhancing the photocatalytic properties of PNIB-AFCC photocatalyst (Table 2, entry 2) for C–S bond formation reaction.

The scope of C–S bond formation was considered for reaction of phenyl acetylene and thiol under the optimized reaction conditions (Table 3, entry 1). As a result, various substituted phenyl/cyclic acetylene were evaluated as reactants for the C-S bond formation. As depicted

TABLE 1 PNIB-AFCC-based LPG sensor attributes

Sensor parameter			
Concentration of LPG (vol%)	% SR	Response time (s)	Recovery time (s)
0.5	147.06	2.44	1.00
1.0	226.47	3.51	1.83
1.5	381.63	3.95	2.88
2.0	635.29	5.82	5.54

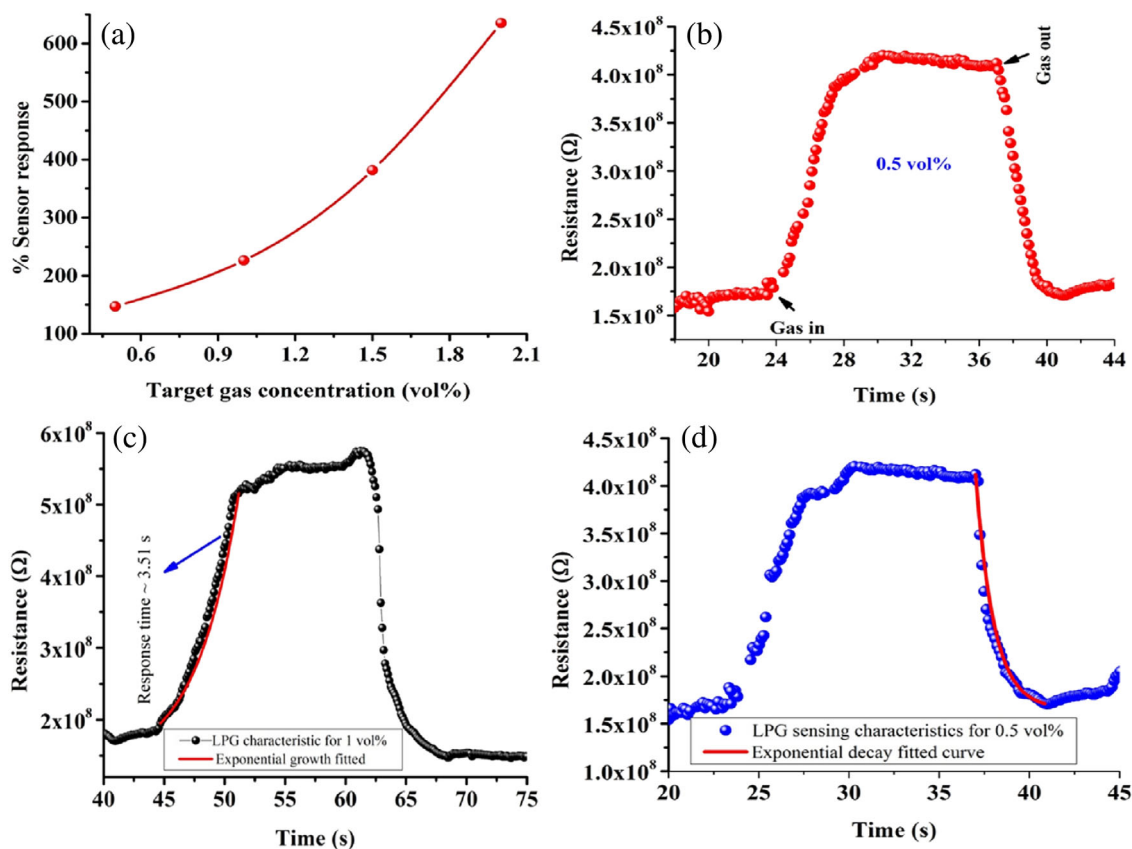
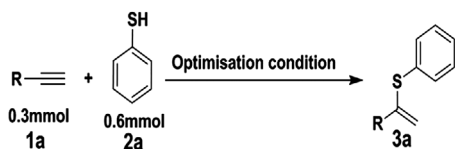


FIGURE 7 LPG sensor attributes of PNIB-AFCC



Entry	Conditions	Yield[%]	Selectivity[%]
1.	PNIB, Na ₂ CO ₃ (1eq.), DMF, 1h	82	84
2. ^a	PNIB-AFCC Na ₂ CO ₃ (1eq.), DMF, 1h	99	99
3. ^b	PNIB-AFCC, Na ₂ CO ₃ (1eq.), DMF, No light, 12h	0	0
4.	T, Na ₂ CO ₃ (1eq.), DMF, 1h	26	25
5.	AFCC, Na ₂ CO ₃ (1eq.), DMF, 1h	0	0
6. ^c	No photocatalyst, Na ₂ CO ₃ (1eq.), DMF, 12h	0	0
7.	PNIB-AFCC, No base, DMF, 12h	0	0

^aReaction conditions: PNIB-AFCC photocatalyst (1 mol%), thiophenol (0.3 mmol), terminal alkyne (0.6 mmol) Na₂CO₃ (1 eq), DMF (4.0 ml), blue LED light under N₂ atmosphere, 1 hr.

^bWithout irradiation of light.

^cWithout using photocatalyst.

in Table 3, the reaction with phenyl acetylene with thiol gives the expected vinyl sulfide products (phenyl [1-phenylvinyl] sulfane) in 99% yield with outstanding 99% reactant conversion (Table 3, entry 1, Figure S9). Significantly 1-ethynyl-1-cyclohexanol also gives product (1-(1-[phenylthio]vinyl)cyclohexanol) in 97% yield with 97% reactant conversion (Table 3, entry 2, Figure S10), and 4-ethynyl biphenyl yield 98% with 98% conversion (Table 3, entry 3, Figure S11) of reactant in product (1-[biphenyl-4-yl]vinyl)(phenyl)sulfane), which was also confirmed by ¹H NMR spectroscopy (see Figure S8). These following experiments show outstanding light harvesting and photocatalytic property of PNIB-AFCC photocatalyst.

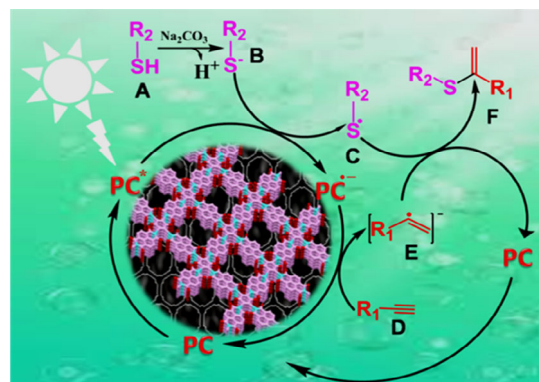
On the basis of these experiments, a possible mechanism of solar light-induced radical-radical addition of sulfide radical (C) and α -vinyl carbon radical (E) is shown in Scheme 3. Initially, S-nucleophile (B) is generated from acid-base neutralization reaction between thiophenol (A) and base. Consequently, the excited state of photocatalyst (PC*) reacts with B to give intermediate C along with the formation of radical anionic photocatalyst (PC^{•-}). Then, photocatalyst (PC^{•-}) reacts with terminal alkyne (D) to induce the formation of an α -vinyl carbon radical intermediate E. After that radical-radical coupling product F is formed through the radical reaction and proton transfer mechanism.

3 | EXPERIMENTAL

3.1 | Material

Tetrachloro-*p*-benzoquinone (TCB), naphthalene-1, 4, 5, 8-tetracarboxylic dianhydride, acetonitrile (ACN),

TABLE 2 Optimization conditions for C–S bond formation reaction under solar light irradiation



SCHEME 3 Plausible mechanisms for the radical-radical coupling reaction of terminal alkyne and thiol

potassium phthalimide, hydrazine hydrate, DMF, thiophenol, phenylacetylene, 1-ethynyl-1-cyclohexanol, 4-ethynyl biphenyl, were purchased from Sigma-Aldrich and TCI Chemicals.

3.2 | Synthesis of PNIB and PNIB-AFCC photocatalysts

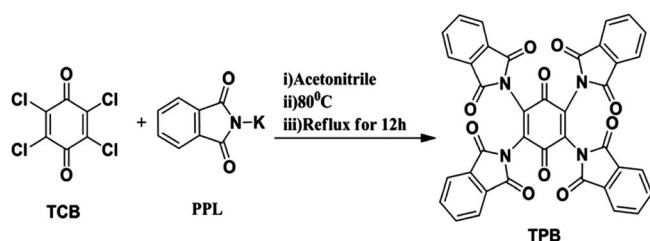
3.2.1 | Step 1: Synthesis of tetra(phthalimido)-benzoquinone (TPB)

Tetra(phthalimido)-benzoquinone (TPB) was prepared by following the well-established method.^[33] First, TCB 5 g and potassium phthalimide 15.0 g were mixed in 50.0 ml of ACN. After that the solution was reflux under inert atmosphere at 80°C for 16 hours. After the completion of reaction, the solution was removed from the oil bath, and

TABLE 3 Substrate scope of regioselective for C–S bond formation reaction

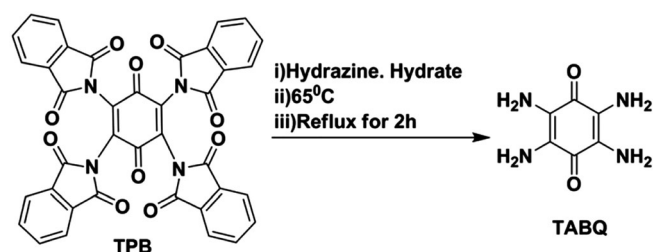
Entry	Substrate	Product	Yield(%)	Selectivity(%)
1.			99	99
2.			97	97
3.			98	98

then cooled solution was filtered. Filtrate was washed with DMF and copious amount of hot deionized water. Finally, the obtained product was suspended in 200 ml of ethanol at 78°C, and then was filtered. Filtrate was then dried in oven at 105°C for 12 hours. Finally, we obtain 5 g of brown-colored TPB compound.



3.2.2 | Step 2: Synthesis of tetraamino-benzoquinone

The as-prepared TPB was mixed with 250.0 ml of hydrazine hydrate and equipped with 500 ml of round bottom flask. After that, reflux it at 65°C for 2 hours, the obtained product is brown-colored tetraamino-benzoquinone (TABQ).



3.2.3 | Step 3: Synthesis of activated flexible carbon cloth

Activated carbon cloth was prepared by the reported literature method.^[44] Firstly, we take pieces of carbon cloth, wash it with acetone and huge amount of water for a number of times. After that the washed cloth was treated with conc. HNO₃ at 100°C for 4 hr. Finally, the acid-treated carbon cloth was washed with distilled water followed by acetone and dried in oven overnight at 50°C. Lastly, we obtain activated flexible carbon cloth for photocatalytic reaction.

3.2.4 | Step 4: Synthesis of PNIB and PNIB-AFCC photocatalysts

About 15.6 mg of TABQ (T), 50.0 mg N, and 250 mg of activated flexible carbon cloth were mixed into 20.0 ml of DMSO solution. Mixture was added to an N₂-filled 250-ml two-neck round bottom flask equipped with a magnetic stirring bar along with condenser. After that the round bottom flask was placed in an oil bath and refluxed at 180°C for 2 days. The obtain product was washed with huge amount of water, and acetone. Finally, the obtained product PNIB-AFCC photocatalyst was dried in oven. The PNIB photocatalyst was prepared via the same synthetic route without the addition of activated flexible carbon cloth. The chemical structure of PNIB photocatalyst (see Figure S1) was confirmed by both liquid¹H and solid-state¹³C nuclear magnetic resonance (NMR) spectroscopy (Figure S12), elemental analysis (Table S1), and Fourier-transform infrared spectroscopy (Figure S13).

4 | CONCLUSIONS

In this study, we have developed a newly designed PNIB-AFCC photocatalyst for C–S bond formation under solar light irradiation. With the help of microscopy, thermal analysis, and spectroscopy, the as-prepared PNIB and PNIB-AFCC photocatalysts have been characterized. Electron-transfer mechanism and photocatalytic activity of photocatalyst was studied through cyclic voltammetry. Due to the presence of light harvesting properties, suitable band gap, and photocatalytic properties PNIB-AFCC photocatalyst is highly efficient for regioselective C–S bond formation and LPG sensing. The C–S bond containing vinyl sulfides compound has wide applications in medicinal and pharmaceutical chemistry.

ACKNOWLEDGMENTS

This work was supported by Madan Mohan Malaviya University of Technology (MMMUT), Gorakhpur U.P., India.

ORCID

Rajesh K. Yadav  <https://orcid.org/0000-0002-5320-5259>
Tae Wu Kim  <https://orcid.org/0000-0002-6370-0907>

REFERENCES

- [1] U. Wille, *Chem. Rev.* **2013**, *113*, 813.
- [2] M. Beller, J. Seayad, A. Tillack, H. Jiao, *Angew Chem Int Ed Engl.* **2004**, *28*, 3368.
- [3] J. Cuthbertson, J. D. Wilden, *Tetrahedron* **2015**, *71*, 4385.
- [4] J. D. Cuthbertson, D. W. C. MacMillan, *Nature* **2015**, *519*, 74.
- [5] S. S. Zaleskiy, N. S. Shlapakova, V. P. Ananikov, *Chem. Sci.* **2016**, *7*, 6740.
- [6] J. Yang, A. Sabarre, L. R. Fraser, B. O. Patrick, J. A. Love, *J. Org. Chem.* **2009**, *74*, 182.
- [7] S. Ranjit, Z. Duan, P. Zhang, X. Liu, *Org. Lett.* **2010**, *12*, 4134.
- [8] S. Mao, Y. R. Gao, X. Q. Zhu, D.-D. Guo, Y.-Q. Wang, *Org. Lett.* **2015**, *17*, 1692.
- [9] M. Feng, B. Tang, S. Liang, X. Jiang, *Top. Med. Chem.* **2016**, *16*, 1200.
- [10] G. A. Patani, E. J. LaVoie, *Chem. Rev.* **1996**, *96*, 3147.
- [11] E. A. Iardi, E. Vitaku, J. T. Njardarson, *J. Med. Chem.* **2014**, *57*, 2832.
- [12] D. A. Boyd, *Int. Ed. Angew. Chem.* **2016**, *55*, 15486.
- [13] A. S. Rahate, K. R. Nemade, S. A. Waghuley, *Rev. Chem. Eng.* **2013**, *29*, 471.
- [14] F. Y. Kwong, S. L. Buchwald, *Org. Lett.* **2002**, *4*, 3517.
- [15] M. Murata, S. L. Buchwald, *Tetrahedron* **2004**, *60*, 7397.
- [16] M. A. Fernández-Rodríguez, Q. Shen, J. F. Hartwig, *J. Am. Chem. Soc.* **2006**, *128*, 2180.
- [17] E. Alvaro, J. F. Hartwig, *J. Am. Chem. Soc.* **2009**, *131*, 7858.
- [18] M. Sayah, M. G. Organ, *Chem. Eur. J.* **2011**, *17*, 11719.
- [19] P. Gogoi, S. Hazarika, M. J. Sarma, K. Sarma, P. Barman, *Tetrahedron* **2014**, *70*, 7484.
- [20] D. A. MacMillan, D. W. C. Nicewicz, *Science* **2008**, *322*, 77.
- [21] M. A. Ischay, M. E. Anzovino, J. Du, T. P. Yoon, *J. Am. Chem. Soc.* **2008**, *130*, 12886.
- [22] J. M. R. Narayanam, J. W. Tucker, C. R. J. Stephenson, *J. Am. Chem. Soc.* **2009**, *131*, 8756.
- [23] Y. Zhou, Z. Xiang, D. Cao, C.-J. Liu, *Chem. Commun.* **2013**, *49*, 5633.
- [24] R. Gomes, P. Bhanja, A. Bhaumik, *Chem. Commun.* **2015**, *51*, 10050.
- [25] R. K. Yadav, J.-O. Baeg, A. Kumar, K. J. Oh, G. H. Kong, N. J. Park, *J. Mater. Chem. A* **2014**, *2*, 5068.
- [26] Z. Xiang, D. Caob, L. Dai, *Polym. Chem.* **2015**, *6*, 1896.
- [27] B. C. Patra, S. Khilari, R. N. Manna, S. Mondal, D. Pradhan, A. Pradhan, A. Bhaumik, *ACS Catal.* **2017**, *7*, 6120.
- [28] Z. Liu, J. Ou, H. Wang, X. You, M. Ye, *ACS Appl. Mater. Interfaces* **2016**, *8*, 32060.
- [29] H. D. Jang, S.-K. Kim, S.-J. Kim, *J Nanoparticle Res* **2001**, *3*, 141.
- [30] S. J. Hong, H. Jun, P. H. Borse, J. S. Lee, *Int J Hydrogen Energy* **2009**, *34*, 3234.
- [31] W. Yan, C. Wang, J. Tian, G. Zhu, L. Ma, Y. Wang, R. Chen, Y. Hu, L. Wang, T. Chen, J. Ma, Z. Jin, *Nat Commun* **2019**, *10*, 2513.
- [32] E. R. Tribonia, M. F. P. D. Silva, A. T. Fincoa, M. A. Rodrigues, G. J. F. Demets, F. H. Dyszy, P. C. Isolanía, P. B. Filho, M. J. Politi, *Mater Res* **2010**, *13* 4, 505.
- [33] Z. Luo, L. Liu, J. Ning, K. Lei, Y. Lu, F. Li, J. Chen, *Angew Chem Int Ed Engl.* **2018**, *57*, 9443.
- [34] Y. Chen, H. Li, M. Tang, S. Zhuo, Y. Wu, E. Wang, S. Wang, C. Wang, W. Hu, *J. Mater. Chem. A* **2019**, *7*, 20891.
- [35] D. Yadav, S. K. Awasthi, *Dalton Trans.* **2020**, *49*, 179.
- [36] K. Nagaveni, G. Sivalingam, M. S. Hegde, G. Madras, *Appl Catal B Environ* **2004**, *48*, 83.
- [37] M. Wisniewska, I. Ostolska, D. Sternik, *J Therm Anal Calorim.* **2016**, *125*, 1171.
- [38] K. Kumar, U. Kumar, M. Singh, B. C. Yadav, *J Mater Sci Mater Electron* **2019**, *30*, 13013.
- [39] M. Singh, B. C. Yadav, A. Ranjan, R. K. Sonker, M. Kaur, *Sensors Actuators B Chem* **2017**, *249*, 96.
- [40] K. Kumar, A. Singh, U. Kumar, R. K. Tripathi, B. C. Yadav, *J Mater Sci Mater Electron* **2020**, *31*, 10836.
- [41] M. Singh, B. C. Yadav, A. Ranjan, M. Kaur, S. K. Gupta, *Sensors Actuators B Chem* **2017**, *241*, 1170.
- [42] U. Kumar, B. C. Yadav, *J Taiwan Inst Chem Eng* **2019**, *96*, 652.
- [43] H. Wang, Q. Lu, C. W. Chiang, Yi. Luo, J. Zhou, G. Wang, A. Lei, *Angew. Chem* **2017**, *56*, 595.
- [44] A. Indra, U. Paik, T. Song, *Angew. Chem. Int. Ed.* **2018**, *57*, 1241.

SUPPORTING INFORMATION

Additional supporting information may be found online in the Supporting Information section at the end of this article.

How to cite this article: Singh P, Yadav RK, Kim TW, et al. Solar light active flexible activated carbon cloth-based photocatalyst for Markovnikov-selective radical-radical cross-coupling of S-nucleophiles to terminal alkyne and liquefied petroleum gas sensing. *J Chin Chem Soc.* 2021; 1–10. <https://doi.org/10.1002/jccs.202000374>